# Atmospheric waves and their possible effect on the thermal structure of Saturn's thermosphere

I. C. F. Müller-Wodarg[1], T. T. Koskinen[2], L. Moore[3], J. Serigano[4], R. V. Yelle[2], S. Hörst[4], J. H. Waite[5], and M. Mendillo[3]



This article has been accepted for publication and undergone full peer review but has not been through the copyediting, typesetting, pagination and proofreading process, which may lead to differences between this version and the Version of Record. Please cite this article as doi: 10.1029/2018GL081124

Atmospheric waves have been discovered for the first time in Saturn's neutral upper atmosphere (thermosphere) with typical vertical wavelengths ranging from 100–200 km and density amplitudes reaching around 10%. Amplitudes are roughly constant over this height range, implying that wave damping occurs, which in turn is expected to enhance eddy friction (Rayleigh drag) within the thermosphere. Using the Saturn Thermosphere Ionosphere Gen-

I. C. F. Müller-Wodarg, i.mueller-wodarg@imperial.ac.uk

[1]Blackett Laboratory, Imperial College London, Prince Consort Road, London SW7 2AZ, UK.

[2]Lunar & Planetary Laboratory, University of Arizona, Tucson, AZ, USA.

[3]Center for Space Physics, Boston University, Boston MA, USA.

[4]Department of Earth and Planetary Sciences, Johns Hopkins University, Baltimore MD, USA.

[5]Southwest Research Institute, San Antonio, TX, USA.

eral Circulation Model (STIM), we explore the response of Saturn's thermosphere to a range of possible Rayleigh drag profiles. We find that the introduction of momentum dissipation equatorward of ±60° latitude will slow down the zonal winds on Saturn sufficiently to enhance equatorward winds and thereby allow energy propagation from the poles towards the equator. Under the assumption that sufficiently strong Rayleigh drag is present in Saturn's thermosphere, large temperatures at low latitudes may result from wind driven global redistribution of energy from the polar regions.

**Keypoints:**

- Atmospheric waves have for the first time been detected in-situ in Saturn's thermosphere by the Cassini INMS during the final proximal orbits
- A drag force associated with wave breaking alters the global winds and temperatures
- Enhanced equatorward winds transport energy from magnetosphere-atmosphere coupling at the poles towards the equator, explaining the large observed temperatures

## 1. Introduction

Our inability to explain the high thermosphere temperatures observed at low latitudes on Jupiter and Saturn [*Yelle and Miller*, 2004] highlights a fundamental lack of understanding of the energy balance in giant planet atmospheres. To-date, studies have examined the effects of direct heating by dissipating gravity or acoustic waves [*Young et al.*, 1997; *Schubert et al.*, 2003; *O'Donoghue et al.*, 2016] but found that even under optimal conditions, wave heating could only provide part of the missing energy at low latitudes [*Matcheva and Strobel*, 1999; *Hickey et al.*, 2000; *Strobel*, 2002; *Yelle and Miller*, 2004]. Motivated by temperature retrievals from Cassini observations [*Koskinen et al.*, 2013, 2015] as well as recent in-situ observations by Cassini's Ion and Neutral Mass Spectrometer [*Yelle et al.*, 2018], we revisit the question and investigate the role of additional horizontal Rayleigh drag on the global circulation and temperatures of the upper atmosphere using the Saturn Thermosphere Ionosphere General Circulation Model [*Müller-Wodarg et al.*, 2006a, 2012].

At high latitudes, magnetosphere-ionosphere interactions maintain the high temperatures. All giant planets in our solar system are surrounded by magnetospheres, large cavities formed by the internal planetary magnetic fields which shield the planets from the direct impact of the solar wind. Following a mechanism first proposed for Jupiter [*Hill*, 1980; *Cowley and Bunce*, 2001], magnetosphere-ionosphere interaction at Saturn causes transfer of angular momentum from the upper atmosphere to the magnetosphere plasma. In addition, solar wind forcing plays a role at Saturn [*Cowley and Bunce*, 2001], as for Earth, but the continuous flow of angular momentum from atmosphere to the mag-

netosphere which dominates at Jupiter is also necessary at Saturn due to the continuous deposition of material from Enceladus and ring material into the magnetosphere. These field-aligned currents lead to precipitation of energetic electrons into the thermosphere near the magnetic poles, generating local ionisation which in the presence of electric fields leads to westward (against the planet rotation) ionospheric plasma jets in the auroral region and intense Joule heating [*Müller-Wodarg et al.*, 2012; *Cowley et al.*, 2004]. The energy supplied to the upper atmosphere via this interaction is around 2 TW on Saturn (100 TW on Jupiter), globally a factor of 10 (125 for Jupiter) times the solar heating energy [*Strobel*, 2002]. Calculations with General Circulation Models (GCMs) have previously suggested that the rapid rotation of Jupiter and Saturn trapped this energy near the poles [*Smith et al.*, 2007; *Müller-Wodarg et al.*, 2006a; *Smith and Aylward*, 2009], leaving equatorial regions cold. While the polar regions are supplied with enough energy to heat the thermosphere globally, the difficulty primarily consisted in the strong zonal winds trapping the energy near the poles, leaving the equatorial regions too cold. We investigate this energy problem for the case of Saturn by examining for the first time the role of wave-induced friction on the global wind system and temperatures.

## 2. Observations

The thermosphere of Saturn has been observed remotely with Ultraviolet (UV) occultations by the Voyager and Cassini spacecraft [*Koskinen et al.*, 2013, 2015; *Vervack and Moses*, 2015] and in polar (auroral) regions by observations of IR radiation by the Cassini spacecraft and ground based telescopes [*Stallard et al.*, 2004; *Melin et al.*, 2011]. These and recent in-situ observations [*Yelle et al.*, 2018] have shown exospheric temperatures on

Saturn to reach values of 340–470 K at low- to mid-latitudes and 470–530 K at latitudes poleward of $40^o$ latitude. When calculating exospheric temperatures on Saturn from solar EUV heating alone, values reach around 180 K over the equator [*Yelle and Miller*, 2004; *Müller-Wodarg et al.*, 2006a], with solar cycle changes being responsible for variations of less than 10 K [*Müller-Wodarg et al.*, 2006a], illustrating that direct solar heating represents only a minor heat source in the upper atmosphere of Saturn. The same applies to Jupiter, Uranus and Neptune [*Yelle and Miller*, 2004], in stark contrast to the situations at Earth, Mars and Venus where solar heating is dominant [*Hedin*, 1987; *Bougher*, 1995].

Recently, the Cassini spacecraft during its Grand Finale "Deep Dip" orbits approached Saturn to around 1600 km above the 1 bar level, allowing the Ion and Neutral Mass Spectrometer (INMS) [*Waite et al.*, 2004] to carry out the first ever in-situ measurements of densities in Saturn's thermosphere.

Figure 1 shows $H_2$ density perturbations with respect to a hydrostatic fit to the densities observed by the INMS during "Deep Dip" orbits 288, 290, 291 and 292. During these orbits, the spacecraft reached down to 1630 km altitude above the 1 bar level near latitude 5°S. In producing the hydrostatic fit, densities along an entire pass through Saturn's atmosphere were initially fit with a curve which assumed the exponential change of density with height, following the procedure previously applied to data from the Venus Express spacecraft [*Müller-Wodarg et al.*, 2016]. The reader is referred to the supporting information for a description of our technique for extracting perturbations from the density dataset. The obtained hydrostatic density profile was subtracted from the measurements, eliminating the exponential altitude trends. Next, larger-scale background trends had to

be removed from the remnants in order to isolate any wave-like periodic features. Through trial and error, we found that a $4^{\text{th}}$ degree polynomial provided the optimal solution, on the one hand eliminating the larger scale background trends along an entire pass while on the other hand not adding any artificial perturbations to the dataset. By subtracting these polynomial fits from the perturbation dataset, we obtained the black dots of residuals shown in Figure 1 (as further discussed in the supporting information). A Fast Fourier Transform was then applied to these residuals and the 8 strongest components were used to produce the solid black lines, representing spectral fits to the measured residuals. In the $2^{\text{nd}}$ and $4^{\text{th}}$ rows of panels, this black line is plotted versus altitude above the 1-bar level for each orbit, separating between the inbound (solid) and outbound (dashed) passes. We furthermore calculated the 1-$\sigma$ variations along the spacecraft trajectories within 10 second bins and plotted these at intervals equivalent to 50 seconds in the same panels as a function of altitude (grey bars). Provided that the signal is significant, the spectral fit curves of all orbits (thick lines in the displays versus time from closest approach) suggest the presence of atmospheric perturbations with amplitudes reaching 5–10%.

In principle, these could be interpreted as either horizontal or vertical variations in the atmosphere since the spacecraft travelled both horizontally (covering a distance of around 21,000 km during the observations presented here) and vertically (over a range of 600 km vertically) through the atmosphere during these observations. As discussed by *Müller-Wodarg et al.* [2006b] for the case of Titan, mapping the major consecutive "peaks" and "troughs" of perturbations as a function of horizontal distance and alternatively as a function of altitude in the atmosphere may give an indication of the orientation of the

waves. For the case of vertical waves, their peaks and troughs would be spaced roughly uniformly in altitude but not when mapped horizontally along the spacecraft orbit, and vice versa for horizontal waves. This distinction cannot be made from our dataset at Saturn due to the large ratio of horizontal to vertical distance covered on Saturn (35:1), leading to shallow spacecraft angles only with respect to the horizontal plane (below 5.5° in magnitude). Hence, both interpretations are possible. If interpreted as vertical waves, the density oscillations have vertical wavelengths of 100–300 km. If interpreted as horizontal waves, their horizontal wavelengths would range from 1550–3500 km. The wavelengths are consistent between the different orbits.

Gravity waves in Saturn's stratosphere and ionosphere have previously been detected remotely [*Harrington et al.*, 2010; *Matcheva and Barrow*, 2012] but this is the first time that these waves have been detected in-situ in the thermosphere. The vertical wavelengths inferred here are similar in magnitude to the vertical scales of electron density variability (165–570 km) detected in Saturn's ionosphere [*Matcheva and Barrow*, 2012] between 500 and 2000 km altitude. The similarity between our vertical wavelengths and the vertical periodicities in the ionosphere lends support towards interpreting our oscillations as vertical waves, though future observations will be needed to help clarify the ambiguity.

What effects could such waves in thermosphere density have on the overall circulation of the thermosphere? The amplitudes of vertically propagating atmospheric waves have a natural tendency to increase with altitude by $1/\sqrt{\rho}$ due to the exponential decrease with altitude of the density $\rho$. In the stratosphere, waves may dissipate and break when their amplitudes reach a critical value and thereby generate turbulence and mean-flow

acceleration [*Lindzen*, 1981]. If waves reach the thermosphere, molecular viscosity and thermal conduction play a dominant role and may offset such an increase in wave amplitude, keeping it constant and leading to a deposition of momentum into the background atmosphere. No increase of wave amplitude with altitude can be identified in Figure 1, suggesting that the waves are damped.

Assuming that dissipation limits the vertical growth of wave amplitudes and keeps it constant, the momentum lost by inertio-gravity waves causes zonal mean acceleration in the background atmosphere which can be expressed as [*Hinson and Magalhães*, 1993]:

$$\frac{\partial \bar{u}}{\partial t} \approx -\frac{N^2 k_h}{2 H k_z^3} \tag{1}$$

where $\bar{u}$ is the mean zonal wind, $N$ is the Brunt-Väisälä frequency ($N \approx 7 \cdot 10^{-3}$ s$^{-1}$ in Saturn's thermosphere at 1600 km), $k_h = 2\pi/\lambda_h$ is the zonal wavenumber ($\lambda_h$ being the zonal wavelength), $H$ is the pressure scale height (around 150–250 km in Saturn's thermosphere) and $k_z$ is the vertical wavenumber of the waves. The amplitude of an undamped wave would increase with altitude by $\sqrt{1/\rho}$, or around a factor of 4, in our case. While the variability of residuals away from closest approach increases in Figure 1 (1$^{\text{st}}$ and 3$^{\text{rd}}$ rows), this appears more likely to be an increase in the data noise and we cannot from the quality of the data unambiguously link this to an increase in wave amplitude. There remains, however, a small possibility that the waves deposit their momentum at higher altitudes than sampled here. In our present context, we use the above expression to estimate the order of magnitude of acceleration expected from waves with the characteristics that we observed.

Equation 1 should be applied to height at which gravity waves break, and since we observe waves in the thermosphere above 1600 km, we assume 1600 km in the following calculations. This value is also supported by simulations of *Matcheva and Barrow* [2012] who found a 200 km gravity wave to reach its peak amplitude near 1600 km, but we may independently estimate how close the observed waves are to their breaking level. *Hinson and Magalhães* [1993] give an upper limit for temperature perturbations of gravity waves before reaching the wave breaking level (their Equation 8). Assuming adiabatic motion, we may infer temperature perturbations from density perturbations via $\delta T/T = (R/c_v)\,\delta\rho/\rho$, allowing us to convert our normalised $H_2$ density perturbations ($\delta n_{\mathrm{H2}}/n_{\mathrm{H2}} \approx \delta\rho/\rho$) of Figure 1 into $\delta T/T$ values. Comparing $\delta T$ to the right side of Equation 8 of *Hinson and Magalhães* [1993], we find the $\delta T$ to be near the breaking limit on all orbits in our observations. Therefore, Equation 1 is indeed likely to be applicable in Saturn's thermosphere near 1600 km.

Assuming the observed waves to be primarily vertical ($\lambda_z = 200$ km, $\lambda_h = 32,000$ km) gives an acceleration of magnitude $\approx 1 \cdot 10^{-3}$ ms$^{-2}$, while assuming them to be primarily horizontal ($\lambda_z = 300$ km, $\lambda_h = 1,600$ km) gives an acceleration of magnitude $\approx 0.1$ ms$^{-2}$. These values translate into around 40 m s$^{-1}$day$^{-1}$ and 4 km s$^{-1}$day$^{-1}$, respectively, where we assumed one day to represent the length of a Saturn rotation (10.66 h). The value estimated for vertical waves is comparable in magnitude to the accelerations calculated in Saturn's thermosphere [*Müller-Wodarg et al.*, 2006a, 2012], implying that such waves could potentially have an important impact on the dynamics of Saturn's upper atmosphere. If we assume a lower wave breaking height than 1600 km, the accelerations increase

asymptotically to around 3.5 times the above values, further emphasising their potential significance in affecting the global circulation.

Momentum deposition by gravity waves and tides was investigated for Earth by *Schoeberl and Strobel* [1978]; *Holton and Wehrbein* [1980]; *Lindzen* [1981] and *Holton* [1982] amongst others who numerically described their effects on the background winds through a simple Rayleigh friction term ($\partial u/\partial t \approx -\alpha u$) which acted to reduce the zonal flow, $u$, in models of Earth's mesosphere in an effort to reproduce the observed temperature structure there. Given the scarcity of available gravity wave and tidal observations at the time of these early studies, comparable to our current state of knowledge at Saturn, the Rayleigh friction parameter, $\alpha$, was inferred empirically by matching simulated winds and temperatures with observations. We will in the following pursue a similar path for Saturn's thermosphere, with the aim of developing a more sophisticated and realistic gravity wave momentum deposition scheme in the future.

## 3. The STIM model and simulations

The Saturn Thermosphere Ionosphere General Circulation Model (STIM) represents the first 3-D GCM published for Saturn's upper atmosphere, making it an ideal tool for investigating the global circulation and associated thermal structure on Saturn. STIM numerically integrates the time-dependent coupled Navier-Stokes equations of momentum, energy and continuity for neutral gases and ions on a global spherical pressure grid. It calculates solar radiation heating and ionisation as well as auroral electron impact ionisation and magnetospheric electric fields mapping into high latitudes along the magnetic field lines [*Müller-Wodarg et al.*, 2012; *Moore et al.*, 2010; *Galand et al.*, 2011; *Jia et al.*,

2012]. The effects of atmosphere-magnetosphere coupling on the atmosphere are treated self-consistently in STIM through high latitude ion drag and Joule heating. The high latitude electric field and region of electron precipitation are defined by simulations from the BATSrUS model [*Jia et al.*, 2012].

The studies of *Müller-Wodarg et al.* [2006a] and *Smith et al.* [2007] have shown that the energy from Joule heating near the poles of a fast spinning giant planet is blocked from being distributed towards the equator due to strong Coriolis forces in the atmosphere, forming a "Coriolis barrier" of primarily zonal winds.

Like for the case of Earth, circulation models of the thermosphere of Venus also did not originally reproduce the correct temperature structure. This difficulty was resolved by invoking an extra Rayleigh friction term to represent friction from smaller scale turbulent processes not resolved by the codes [*Bougher et al.*, 1986, 1988]. It is therefore unsurprising that a similar approach may be necessary for Saturn and possibly the other giant planets as well. We investigate the sensitivity of winds and temperatures in Saturn's thermosphere to various global profiles of Rayleigh friction.

To investigate the possible effects of wave-induced Rayleigh friction on the thermal structure in Saturn's thermosphere, we introduce into the horizontal momentum equation of STIM [*Müller-Wodarg et al.*, 2006a] an additional Rayleigh drag term, $\vec{a}_{\rm drag}$ (in ms$^{-2}$) based on that of *Bougher et al.* [1986, 1988] and given by:

$$\vec{a}_{\rm drag} = -\vec{U}\ \Lambda(\theta)\ \alpha\ \left(1+\sqrt{\frac{p_0}{p}}\right)^{-1} \tag{2}$$

where $\vec{U} = u\ \hat{\Phi} + v\ \hat{\theta}$ is the horizontal 2-D wind vector with the zonal ($u$) and meridional ($v$) wind speed components ($\hat{\Phi}, \hat{\theta}$ being the respective unit vectors), $\alpha = 10^{-3}$ s$^{-1}$ is our

friction parameter and $p_0 = 10^{-4}$ Pa. At $p = p_0$ the bracket term in Equation 2 is 0.5, it monotonically increases to 1 for $p > p_0$ and decreases towards 0 for $p < p_0$. The numerical values of $\alpha$ and $p_0$ were determined empirically from numerous STIM simulations and lead to frictional deceleration values remarkably similar to those estimated from Equation 1. The value for $p_0$ lies in the middle of the pressure range of our model (0.4–3.5·$10^{-7}$ Pa) near the ionosphere peak, at 1500 km above the 1-bar level, slightly below the bottom height sampled during INMS observations of Figure 1. The INMS data of Figure 1 also suggest that wave damping begins to play a role at or below 1700 km altitude, giving an independent justification for the value.

In addition to having a vertical dependency in the drag term via the final term of Equation 2, we also added horizontal (latitudinal) structure by introducing $\Lambda(\theta)$, a dimensionless factor between 0 and 1 which changes with latitude $\theta$. A globally uniform Rayleigh drag term similar in form to Equation 2, without the $\Lambda(\theta)$, is used in the Venus thermosphere GCM of *Bougher et al.* [1986, 1988] to obtain realistic nighttime temperatures. While in the Venus GCM the pressure ratio was written as $\sqrt{p/p_0}$ [*Bougher et al.*, 1988], we apply the term at a higher region (lower pressure) in Saturn's atmosphere and found that the original form of the term increased with altitude and severely damped the thermospheric winds higher up. We instead replaced it with $\sqrt{p_0/p}$ in order to reduce the drag to zero at high altitudes. A physical justification for this approach is that viscous damping will increasingly have extracted wave momentum towards higher altitudes, so any wave–associated Rayleigh drag should diminish with altitude as well.

Note that the expression in Equation (2) acts much like a viscosity term, reducing wind speeds, and will be associated with atmospheric waves having low or zero phase speeds. Our numerical experiments with STIM aim to answer the question of how large Rayleigh friction would need to be in order to have a noticeable effect on the thermosphere winds and temperatures. Future studies will examine whether waves in Saturn's thermosphere are consistent with this Rayleigh friction.

By experimenting with a range of different profiles of $\Lambda(\theta)$ in the expression of Rayleigh drag of Equation 2, we examine the response of Saturn's upper atmosphere to different global distributions of atmospheric drag. We will present four representative cases but examined numerous other cases not shown here.

Figure 2 presents a range of representative $\Lambda(\theta)$ profiles defining the latitudinal change of the Rayleigh drag term of Equation 2 (bottom panel) and the resulting calculated exospheric temperatures (upper panel). All simulations in Figure 2 assume equinox conditions. Simulation E (black) assumes no Rayleigh drag and illustrates the previously noted behaviour found in GCMs such as STIM of Joule heating raising the temperatures near the poles and the primarily zonal circulation in the atmosphere trapping this energy there, leaving the equatorial region too cold [*Müller-Wodarg et al.*, 2006a; *Smith et al.*, 2007].

In simulation A (red) we obtain enhanced temperatures at all latitudes compared with the simulation without drag (E, black), but an equator-to-pole temperature difference that is still larger than observed. In this simulation, the change of global atmospheric circulation leads to adiabatic cooling and a temperature decrease of up to 150 K at high

latitudes in the deeper thermosphere near the ionospheric peak ($10^{-4}$ Pa, not shown) and a general increase of temperature at all latitudes in the upper thermosphere due to adiabatic heating at low to mid latitudes and meridional wind transport at polar latitudes. Therefore, exospheric temperatures in Simulation A appear enhanced everywhere, though this is only due to a vertical redistribution of energy and represents no violation in energy conservation.

Simulation B (blue) gives equatorial and polar temperatures considerably more consistent with observations. Case D (green) represents a $\Lambda(\theta)$ similar to B, but with a more gradual decrease equatorward of 60° latitude, while C (purple) assumes $\Lambda_C = \Lambda_A + \Lambda_D$. The temperatures of C and D are indistinguishable and similar to B. The summed $\chi$-squared values, normalised to that of Simulation B, are 2.7, 1.0, 1.2, 1.3 and 22.9 for Simulations A-E, respectively, and indicate that simulations B, C and D represent the best matches to the observations. The experiments illustrate that additional atmospheric drag at latitudes equatorward of ±65° is needed to obtain temperatures at low latitudes consistent with observations, but that the strength of Rayleigh drag at latitudes equatorward of ±30° matters little for the overall temperature results. We shall in the following use C as our reference drag profile but recognise that B and D give similar results.

By examining the terms of the energy and momentum equations of the model, we find that our Rayleigh drag term roughly balances the Coriolis term in our simulations. As a result, the zonal winds are reduced and meridional winds enhanced, allowing for the equatorward transport of polar thermal energy. Winds are upward at high latitudes and

downward over the equator, causing adiabatic heating at low latitudes. More details are presented in the supporting information.

Figure 3 shows a comparison of measured temperatures (symbols) with STIM simulations (lines) assuming the Rayleigh drag term of Equation (2) and $\Lambda(\theta)$ from Simulation C. Red and blue lines denote southern and northern hemisphere summer conditions, respectively, while green is for equinox. The data points have been coloured such that red, green and blue represent conditions where Saturn's solar declination angle, $\xi$, was $\xi \leq -10^{\mathrm{O}}$, $-10^{\mathrm{O}} < \xi < 10^{\mathrm{O}}$ and $\xi \geq 10^{\mathrm{O}}$, respectively, roughly matching the seasonal conditions of the three lines from simulations. The blue line corresponds to the seasonal conditions during Cassini's final orbits and it matches the observations corresponding to this season reasonably well, with the exception of southern high latitudes where the observed temperature is cooler. Overall, the model predicts hotter temperatures at mid-to high latitudes in the summer hemisphere (compared with the winter hemisphere). The seasonal behaviour seen in these simulations is due to higher insolation and electron densities in the summer that lead to enhanced high-latitude resistive (Joule) heating there. Seasonal changes in the thermosphere should therefore be strongly modulated by the ionosphere, which acts as the interface between magnetosphere and the thermosphere. Direct solar heating causes negligible seasonal changes in Saturn's thermosphere. However, the seasonal changes of solar ionisation rates generate larger ionospheric plasma densities in the summer hemisphere. In the summer polar region, Joule heating rates are therefore higher than in the winter polar region, leading to differences in temperatures between the poles which are distributed by winds towards lower latitudes as well.

The occultation data points at high latitudes are consistent with this simulation result, although only a few such data points have been published at this point. The data obtained during the Grand Finale orbits include many new high-latitude occultations that will allow us to properly test predictions of seasonal trends. Near the equator, seasonal changes in the exospheric temperature are not easily distinguishable in the observations, in agreement with our simulations. Note, however, that evidence for seasonal variations in temperature at higher pressures near the equator has been obtained from the occultation data [*Koskinen et al.*, 2015]. At mid-latitudes, the scarcity of the observations and the relatively low amplitude of the predicted temperature changes prevent us from drawing firm conclusions regarding seasonal variations. Overall, STIM temperatures at low latitudes exceed observed values by up to around 50 K, so the assumed Rayleigh drag factor represents an upper limit and can in cases be reduced.

## 4. Discussion

In the Earth's mesosphere, dissipating and breaking gravity waves strongly alter the momentum balance and affect the global circulation, explaining the cold summer mesopause temperatures [*Holton and Wehrbein*, 1980; *Holton*, 1982; *Liu et al.*, 2009]. General Circulation Models are well known to not fully capture processes such as the propagation of gravity waves and interaction with the background atmosphere, all of which cause Rayleigh drag whose neglect in circulation models leads to wrong predictions of winds and temperatures. The principle of such additional Rayleigh drag fundamentally affecting the global wind system is well known on both Venus and Earth and now investigated for the first time for the thermosphere of a giant planet.

The recent observations by the Cassini INMS have illustrated that waves are present in Saturn's thermosphere, in accordance also with the situation on Jupiter [*Young et al.*, 1997]. We have with Equation 1 carried out a simple order of magnitude assessment of the acceleration that may be experienced by the background atmosphere due to wave damping. By determining that the observed waves are near their breaking level, we could justify the use of Equation 1 to estimate the dissipation associated with the waves. Applying this damping in our model helped unlock the "Coriolis barrier" that trapped energy near the poles. Other possible contributions to Rayleigh drag include atmospheric small scale turbulence from horizontal wind shears not resolved in our model.

Our calculations have opened up a new approach towards solving the "energy crisis" of giant planet upper atmospheres. Rather than looking at direct heating from waves as an explanation for the high temperatures of giant planet thermospheres, as previously proposed [*Young et al.*, 1997; *Matcheva and Strobel*, 1999], we have explored the idea of extra Rayleigh drag affecting thermosphere temperatures. The energy that raises the temperatures derives from magnetosphere-atmosphere coupling at polar latitudes, the role of Rayleigh drag lies in altering the global winds sufficiently to allow equatorward transport of this energy on a fast spinning planet. Our calculations strongly illustrate that winds and temperatures are intimately coupled in giant planet atmospheres and that temperature observations may help constrain thermospheric winds and the strength of Rayleigh friction in their thermospheres.

**Acknowledgments.** The authors are immensely grateful to the reviewers who with their constructive comments have greatly helped improve this paper. TTK acknowledges

support by the NASA CDAP grant NNX15AN20G. LM acknowledges support from the NASA CDAP grant NNX16AI34G. MM acknowledges support from the NSF INSPIRE grant on Comparative Ionospheres. The Cassini INMS data presented in this paper will be published on the Planetary Data System. Data values displayed in the figures are also available as downloadable ASCII files.



## References

Barrow, D., and K. I. Matcheva (2011). Impact of atmospheric gravity waves on the jovian ionosphere, *Icarus*, 211, 609–622.

Bougher, S. W., R. E. Dickinson, E. C. Ridley, R. G. Roble, A. F. Nagy, and T. E. Cravens (1986). Venus mesosphere and thermosphere. II - Global circulation, temperature, and density variations, *Icarus*, 68, 284–312.

Bougher, S. W., R. G. Roble, R. E. Dickinson, and E. C. Ridley (1988). Venus mesosphere and thermosphere. III - Three-dimensional general circulation with coupled dynamics and composition, *Icarus*, 73, 545–573.

Bougher, S. W. (1995). Comparative thermospheres Venus and Mars, *Adv. Sp. Res.*, 15, (4)21–(4)45.

Cowley, S. W. H., and E. J. Bunce (2001). Origin of the main auroral oval in Jupiter's coupled magnetosphere-ionosphere system, *Planet. Sp. Sci.*, 49, 1067–1088.

Cowley, S. W. H., E. J. Bunce, and J. M. O'Rourke (2004). A simple quantitative model of plasma flows and currents in Saturn's polar ionosphere, *J. Geophys. Res.*, 109, A05212.

Galand, M., L. Moore, I. C. F. Müller-Wodarg, and M. Mendillo (2011). Response of Saturn's auroral ionosphere to electron precipitation: electron density, electron temper-

ature, and electrical conductivity. *J. Geophys. Res.*, doi: 10.1029/2010JA016412.

Harrington, J., R. G. French, and K. I. Matcheva (2010). The 1998 November 14 Occultation of GSC 0622-00345 by Saturn. II. Stratospheric Thermal Profile, Power Spectrum, and Gravity Waves, *Astrophys. J.* 716, 404–416.

Hedin, A. E. (1987). MSIS-86 thermospheric model, *J. Geophys. Res.* 92, 4649–4662.

Hickey, M. P., R. L. Walterscheid, and G. Schubert (2000). Gravity wave heating and cooling in Jupiter's thermosphere, *Icarus* 148, 266–281.

Hill, T. W. (1980). Corotation lag in Jupiter's magnetosphere - Comparison of observation and theory, *Science* 207, 301–302.

Hinson, D. P., and J. A. Magalhães (1993). Inertio-Gravity Waves in the Atmosphere of Neptune, *Icarus* 105, 142–161.

Holton, J. R., and W. M. Wehrbein (1980). A numerical model of the zonal mean circulation of the middle atmosphere, *Pageoph* 118, 284–306.

Holton, J. R. (1982). The role of gravity wave induced drag and diffusion in the momentum budget of the mesosphere, *J. Atmos. Sci.* 39, 791–799.

Jia, X., K. C. Hansen, T. I. Gombosi, M. G. Kivelson, G. Tóth, D. L. DeZeeuw, and A. J. Ridley (2012). Magnetospheric configuration and dynamics of Saturn's magnetosphere: A global MHD simulation, *J. Geophys. Res.* 117, A05225.

Koskinen, T. T., B. R. Sandel, R. V. Yelle, F. J. Capalbo, G. M. Holsclaw, W. E. McClintock, and S. Edgington (2013). The density and temperature structure near the exobase of Saturn from Cassini UVIS solar occultations, *Icarus* 226, 1318–1330.

Koskinen, T. T., B. R. Sandel, R. V. Yelle, D. F. Strobel, I. C. F. Müller-Wodarg, and J. T. Erwin (2015). Saturn's variable thermosphere from Cassini/UVIS occultations, *Icarus* 260, 174–189.

Lindzen, R. S. (1981). Turbulence and stress owing to gravity wave and tidal breakdown, *J. Geophys. Res.* 86, 9707–9714.

Liu, H.-L., D. R. Marsh, C.-Y. She, Q. Wu, and J. Xu (2009). Momentum balance and gravity wave forcing in the mesosphere and lower thermosphere, *Geophys. Res. Lett.* 36, L07805.

Matcheva, K. I., and D. F. Strobel (1999). Heating of Jupiter's Thermosphere by Dissipation of Gravity Waves Due to Molecular Viscosity and Heat Conduction, *Icarus*, 140, 328–340.

Matcheva, K. I., and D. J. Barrow (2012). Small-scale variability in Saturn's lower ionosphere, *Icarus*, 221, 525–543.

Melin, H., T. Stallard, S. Miller, J. Gustin, M. Galand, S. V. Badman, W. R. Pryor, J. O'Donoghue, R. H. Brown, and K. H. Baines (2011). Simultaneous Cassini VIMS and UVIS observations of Saturn's southern aurora: Comparing emissions from H, $H_2$ and $H_3^+$ at a high spatial resolution, *Geophys. Res. Lett.*, 38, L15203, doi:10.1029/2011GL048457.

Moore, L., I. C. F. Müller-Wodarg, M. Galand, A. Kliore, and M. Mendillo (2010). Latitudinal variations in Saturn's ionosphere: Cassini measurements and model comparisons. *J. Geophys. Res.*, 115, A11317.

Müller-Wodarg, I. C. F., M. Mendillo, R. V. Yelle, and A. D. Aylward (2006). A global circulation model of Saturn's thermosphere *Icarus*, 180, 147–160.

Müller-Wodarg, I. C. F., R. V. Yelle, N. Borggren, and J. H. Waite (2006). Waves and horizontal structures in Titan's thermosphere *J. Geophys. Res.*, 111, A12315.

Müller-Wodarg, I. C. F., L. Moore, M. Galand, S. Miller, and M. Mendillo (2012). Magnetosphere-atmosphere coupling at Saturn: 1. Response of thermosphere and ionosphere to steady state polar forcing, *Icarus*, 221, 481–494.

Müller-Wodarg, I. C. F., S. Bruinsma, J.-C. Marty, and H. Svedhem (2016). In situ observations of waves in Venus' polar lower thermosphere with Venus Express aerobraking, *Nature Physics*, 12, 767–771.

O'Donoghue, J., L. Moore, T. S. Stallard, and H. Melin (2016). Heating of Jupiter's upper atmosphere above the Great Red Spot, *Nature* 536, 190–192.

Schoeberl, M. R., and D. F. Strobel (1978) The Zonally Averaged Circulation of the Middle Atmosphere, *J. Atmos. Sci.* 35, 577–591.

Schubert, G., M. P. Hickey, and R. L. Walterscheid (2003). Heating of Jupiter's thermosphere by the dissipation of upward propagating acoustic waves, *Icarus*, 163, 398–413.

Seiff, A., D. B. Kirk, T. C. D. Knight, L. A. Young, F. S. Milos, E. Venkatapathy, J. D. Mihalov, R. C. Blanchard, R. E. Young, and G. Schubert (1997) Thermal structure of Jupiter's upper atmosphere derived from the Galileo probe. *Science*, 276, 102–104.

Smith, C. G. A., A. D. Aylward, G. H. Millward, S. Miller, and L. E. Moore (2007) An unexpected cooling effect in Saturn's upper atmosphere, *Nature* 445, 399–401.

Smith, C. G. A., and A. D. Aylward (2009) Coupled rotational dynamics of Jupiter's thermosphere and magnetosphere, *Ann. Geophys.* 27, 199–230.

Stallard, T., S. Miller, L. M. Trafton, T. R. Geballe, and R. D. Joseph (2004). Ion winds in Saturn's southern auroral/polar region, *Icarus*, 167, 204–211.

Strobel, D. F. (2002). Aeronomic Systems on Planets, Moons, and Comets, in "Atmospheres in the Solar System: Comparative Aeronomy", M. Mendillo, A. Nagy, J. H. Waite, eds. *American Geophys. Union*, 7–22.

Vervack, R. J. and J. I. Moses (2015). Saturn's upper atmosphere during the Voyager era: Reanalysis and modeling of the UVS occultations, *Icarus* 258, 135–163.

Waite, J. H., W. S. Lewis, W. T. Kasprzak, V. G. Anicich, B. P. Block, T. E. Cravens, G. G. Fletcher, W.-H. Ip, J. G. Luhmann, R. L. McNutt, H. B. Niemann, J. K. Parejko, J. E. Richards, R. L. Thorpe, E. M. Walter, and R. V. Yelle (2004). The Cassini Ion and Neutral Mass Spectrometer (INMS) Investigation. *Sp. Sci. Rev* 114, 113–231.

Yelle, R. V. and S. Miller (2004). Jupiter's thermosphere and ionosphere, in "Jupiter: Planet, Satellites & Magnetosphere", F. Bagenal, W. McKinnon, and T. Dowling eds. *Cambridge University Press* 185–218.

Yelle, R.-V., J.. Serigano, T. T. Koskinen, S. M. Hörst, M. E. Perry, R. S. Perryman, and J. H. Waite (2018). Thermal Structure and Composition of Saturn's Upper Atmosphere From Cassini/Ion Neutral Mass Spectrometer Measurements, *Geophys. Res. Lett.* 454, https://doi.org/10.1029/2018GL078454.

Young, L.A., R. V. Yelle, R. E. Young, A. Seiff, and D. B. Kirk (1997). Gravity waves in Jupiter's thermosphere. *Science* 276, 108–111.

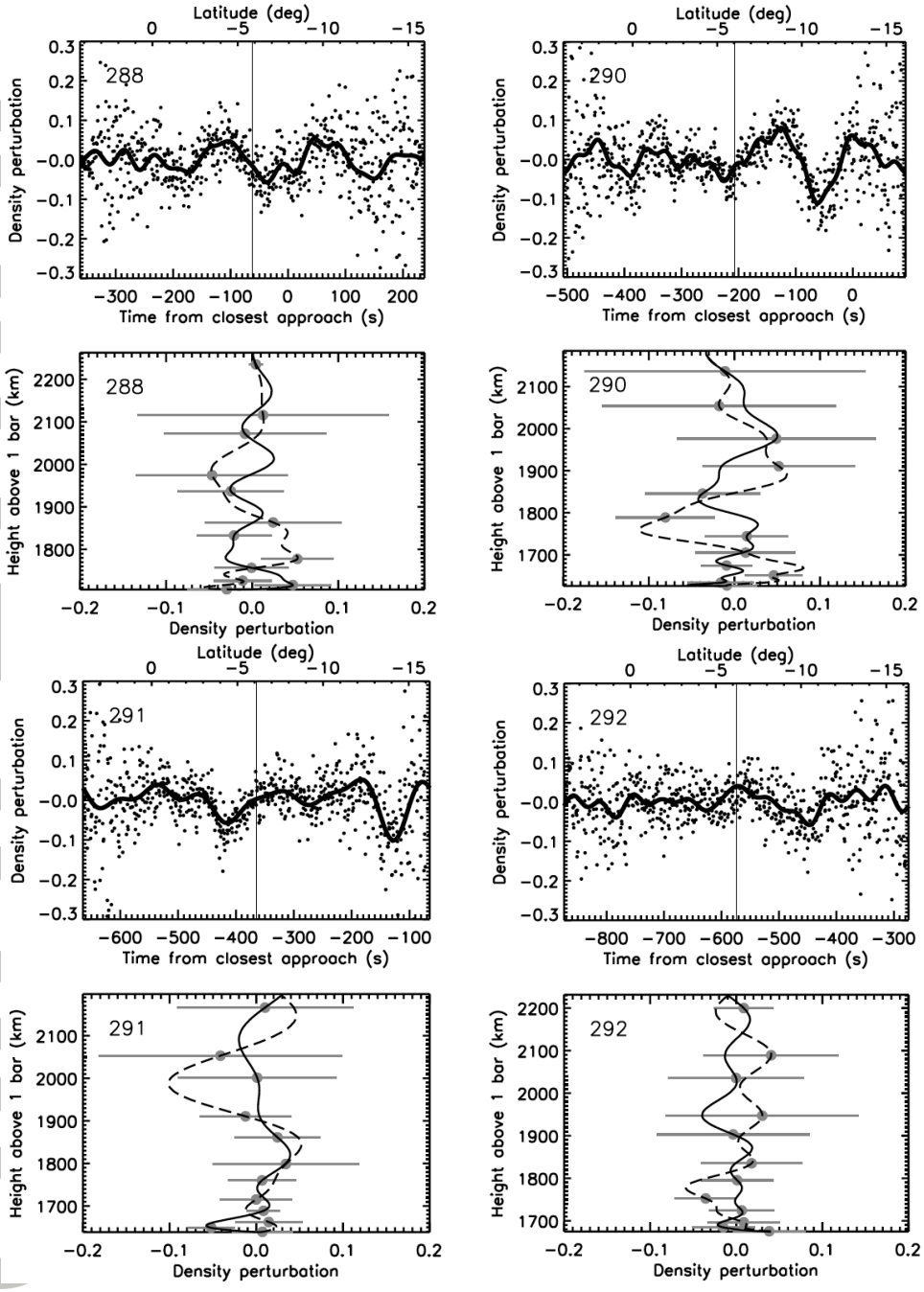


**Figure 1.** $H_2$ density residuals (dots) observed in-situ in Saturn's thermosphere by the Cassini Ion and Neutral Mass Spectrometer (INMS) during "Deep Dip" orbits 288, 290, 291 and 292 on Aug. 14, 27, Sept. 02 and 09, 2017, respectively. The values shown are normalised to the local background densities. The 1$^{st}$ and 3$^{rd}$ rows show values versus time from closest approach, with the black lines denoting a spectral fit to the observations (dots). The 2$^{nd}$ and 4$^{th}$ rows show the spectral fit curves with 1-$\sigma$ error bars (grey) versus altitude above the 1-bar level. Sigma variation bars were calculated from data in 10 sec bins. Solid lines are inbound fits, dashed lines are outbound.

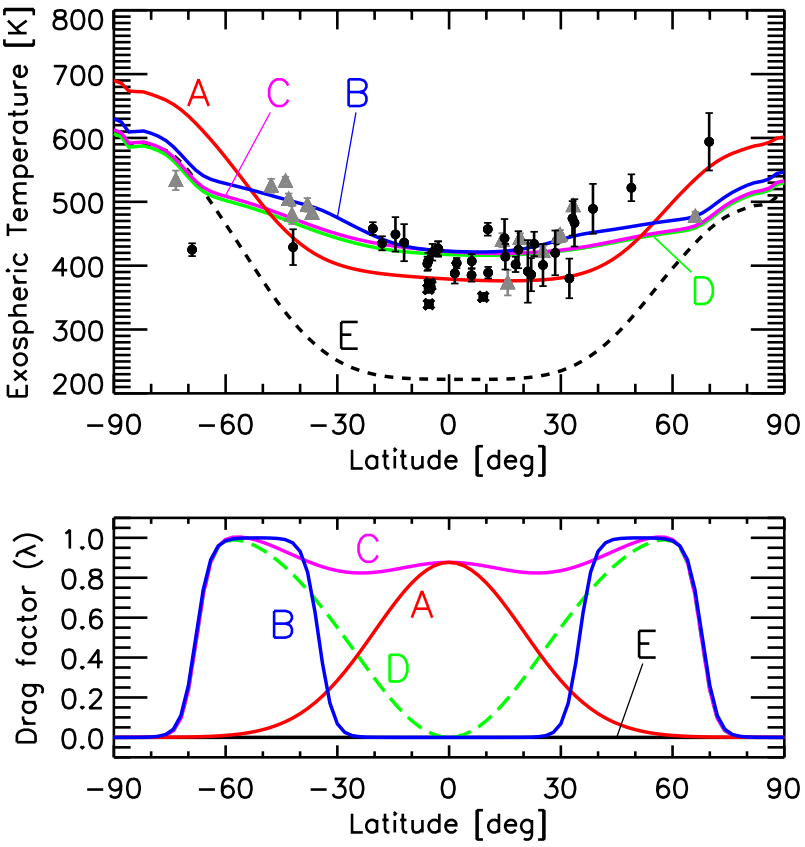


**Figure 2.** Upper panel: Temperatures at the top of Saturn's thermosphere, as observed from stellar (circles) and solar (triangles) UV occultations [*Koskinen et al.*, 2013, 2015] and Cassini INMS in-situ measurements (crosses) [*Yelle et al.*, 2018]. Lines are zonally averaged exospheric temperatures from the Saturn Thermosphere Ionosphere General Circulation Model (STIM) [*Müller-Wodarg et al.*, 2006a, 2012] for equinox conditions. Simulations A-D include the Rayleigh drag term of Equation (2), while E includes no Rayleigh drag. Lower panel: latitudinal profiles of the unitless $\Lambda(\theta)$ term of Equation (2) for the corresponding simulations in the upper panel.

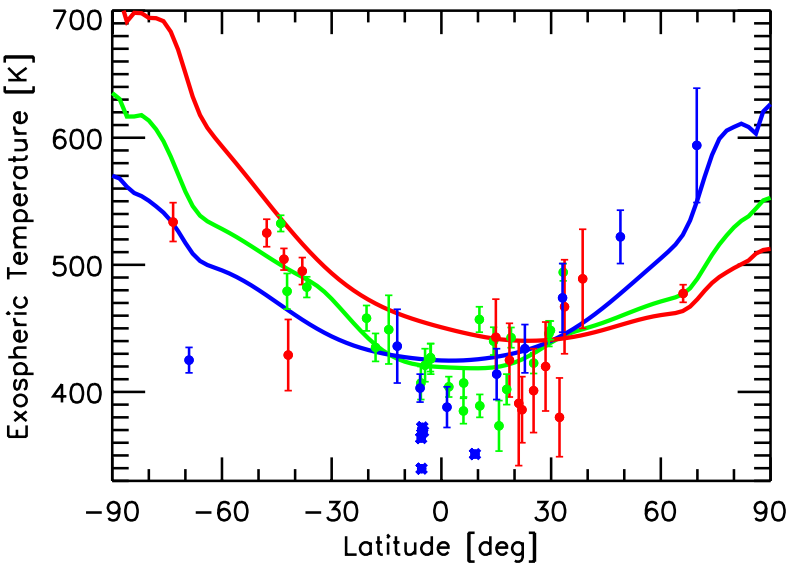


**Figure 3.** Temperatures at the top of Saturn's thermosphere, as observed from UV occultations [*Koskinen et al.*, 2013, 2015] (round symbols), Cassini INMS in-situ measurements [*Yelle et al.*, 2018] (crosses) and calculated by the Saturn Thermosphere Ionosphere General Circulation Model (STIM) [*Müller-Wodarg et al.*, 2006a, 2012], assuming the drag term of Equation (2) with the $\Lambda(\theta)$ from Simulation C (Figure 2, lower panel). Red and blue lines are for southern hemisphere summer and winter conditions, respectively, while the green line is for equinox (Simulation C). Symbol colouring is for solar declination angles $\xi$ of $\xi \geq 10^{\mathrm{O}}$ (blue), $-10^{\mathrm{O}} < \xi < 10^{\mathrm{O}}$ (green) and $\xi \leq -10^{\mathrm{O}}$ (red).